ACS APPLIED ENERGY MATERIALS
Cite This: ACS Appl. Energy Mater. 2019, 2, 2441−2446
Letter
www.acsaem.org

In Situ Focused Ion Beam-Scanning Electron Microscope Study of Crack and Nanopore Formation in Germanium Particle During (De)lithiation

Xinwei Zhou,[†,‡] Tianyi Li,[†] Yi Cui,[†] Melissa L. Meyerson,[§] C. Buddie Mullins,[§] Yuzi Liu,*[,‡] and Likun Zhu*[,†]

[†]Department of Mechanical and Energy Engineering, Indiana University Purdue University Indianapolis, Indianapolis, Indiana 46202, United States

[‡]Center for Nanoscale Materials, Argonne National Laboratory, 9700 South Cass Avenue, Argonne, Illinois 60439, United States

[§]Departments of Chemical Engineering and Chemistry, University of Texas at Austin, Austin, Texas 78712, United States

Supporting Information

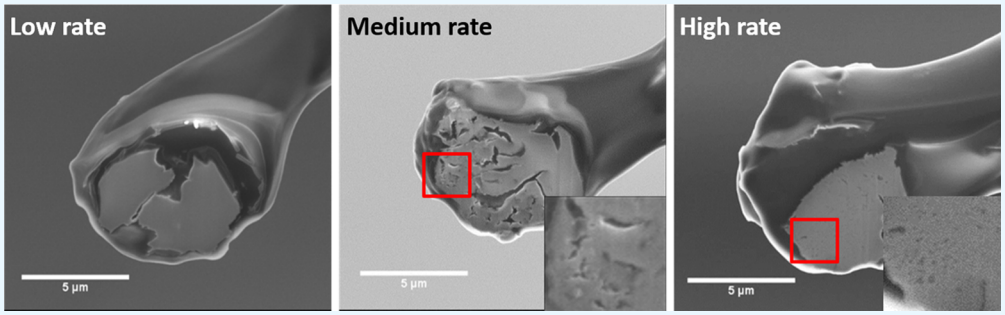

ABSTRACT: Germanium has emerged as a promising high-capacity anode material for lithium ion batteries. To understand the microstructure evolution of germanium under different cycling rates, we monitored single germanium particle batteries using an in situ focused ion beam-scanning electron microscope. Our results show that both the lithium concentration and delithiation rate have an impact on nanopore formation. This study reveals that germanium electrodes with low and high cycling rates have better microstructure integrity, which leads to better cycling performance. The nanopores tend to aggregate into large porous structures during cycling which leads to particle pulverization and capacity fading of the electrode.

KEYWORDS: *lithium ion battery, germanium, nanopore, in situ focused ion beam-scanning electron microscope, pulverization*

Lithium ion batteries (LIBs) have become one of the most important renewable energy storage technologies and have been used in a variety of applications.[1] Currently a graphite anode and metal oxide cathode are commonly used in commercial LIBs. However, the limited capacity and energy density of current LIBs prevent their broader deployment as power sources for high-performance portable electronic devices and electric vehicles.[2−4] Over the past two decades, there has been a continual effort to explore high-capacity electrode materials for LIBs. In addition to graphite (375 mAh g^{-1}), other group IV elements such as silicon (Si), germanium (Ge), and tin (Sn) have drawn significant attention due to their high theoretical capacity.[5,6] Among them, Ge has been considered a promising anode active material, due to its high capacity, low voltage, fast lithium ion diffusion, and high electrical conductivity.[7−9] However, Ge-based anode materials suffer from pulverization due to a large volume change, up to 300%.[7,10] Although pulverization issues can be alleviated by nanostructuring the Ge-based anode materials,[11−15] recent studies have shown that nanometer-sized pores are still formed in the nanostructured electrode due to vacancy-mediated diffusion,[16] which could lead to pulverization during repeated cycling.

In recent years, the reaction mechanism of the Ge anode has been studied by using different in situ and operando characterization methods such as X-ray diffraction (XRD) and X-ray absorption spectroscopy (XAS).[8,17−20] For instance, Lim et al. proposed the phase transformations of Ge that occur during lithiation and delithiation. They also studied the effect of cycling rate on Ge phase transformation during the charge/discharge process and proposed a mechanism to explain the C rate dependence phase transformation phenomenon.[21] However, it is still necessary to correlate the microstructural evolution of the Ge electrode and its electrochemical performance. To this end, some advanced imaging technologies have been used to monitor the microstructural evolution of the Ge electrode during cycling such as transmission

Received: February 22, 2019
Accepted: April 4, 2019
Published: April 4, 2019

DOI: 10.1021/acsaem.9b00380
ACS Appl. Energy Mater. 2019, 2, 2441−2446

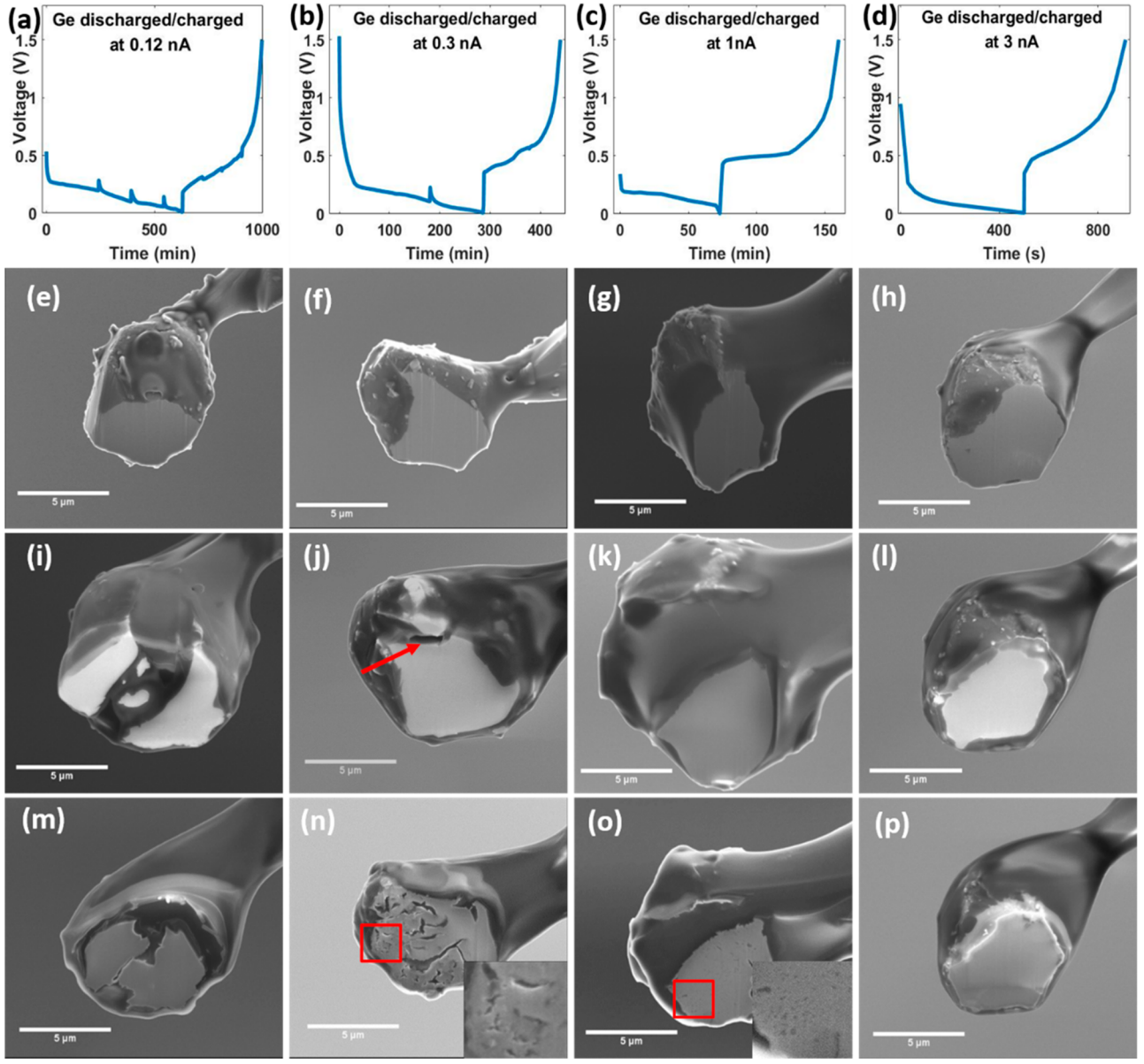

Figure 1. (a–d) Voltage profiles of Ge particles cycled at 0.12, 0.3, 1, and 3 nA. (e–h) SEM images of Ge particles at the as-prepared condition. (i–l) SEM images of Ge particles at the end of lithiation with the four different current rates. (m–p) SEM images of Ge particles at the end of delithiation with the four different current rates. Scale bar is 5 μm.

electron microscopy (TEM)[16,22–24] and transmission X-ray microscopy (TXM).[25] In situ TEM studies have shown the volume expansion during lithiation and formation of nanopores during delithiation in Ge nanowires in real time.[16] However, due to the small size of the sample used in the TEM, it is difficult to control the current rate. In situ TXM can obtain two-dimensional (2D) or three-dimensional (3D) microstructures of Ge particles during cycling with a large field of view. However, the resolution of TXM is not sufficient for monitoring nanometer-sized structures, such as nanopores. Recently, our group has developed an in situ focused ion beam-scanning electron microscope (FIB-SEM) method to study the microstructural evolution of micrometer-sized single Sn particles during lithiation and delithiation.[26] In this study, we used the same *approach* to monitor the microstructure evolution of a Ge particle in a single Ge particle battery and correlate the microstructural evolution to the electrochemical performance change directly.

The experiment was performed on a Zeiss Nvision 40 FIB-SEM at the Center for Nanoscale Materials, Argonne National Laboratory. Figure S1 shows a schematic of the experimental setup. Details of the setup were reported elsewhere.[26] Briefly, micrometer-sized Ge particles were made using the jet mill process shown in ref 27. The ionic liquid electrolyte was made by dissolving the Li salt, lithium bis(trifluoromethylsulfonyl)-imide (LiTFSI) (Sigma-Aldrich), in a solvent of 1-butyl-1-methylpyrrolidinium bis(trifluoromethylsulfonyl)imide (P14TFSI) (Sigma-Aldrich). A Keithley 6430 subfemtoamp remote sourcemeter was used to control the current. During cycling, the Ge particle was immersed in electrolyte. At different states of charge, the cycling was stopped, and the particle was lifted out of the electrolyte for imaging. Residual electrolyte remaining on the particle was removed by FIB

DOI: 10.1021/acsaem.9b00380
ACS Appl. Energy Mater. 2019, 2, 2441–2446

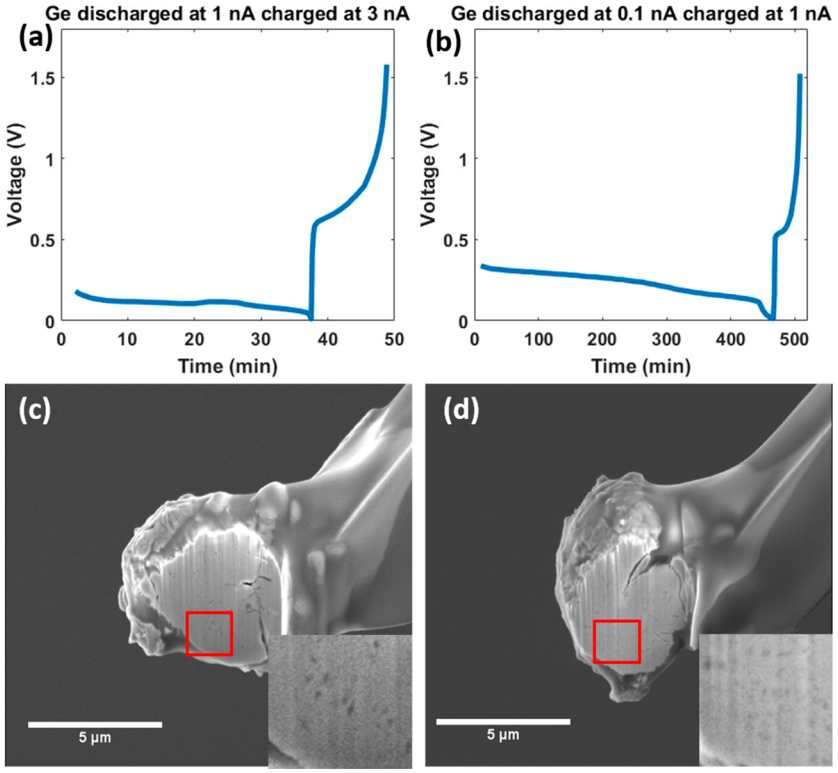

Figure 2. (a) Voltage profile of a Ge particle lithiated at 1 nA and delithiated at 3 nA. (b) Voltage profile of a Ge particle lithiated at 0.1 nA and delithiated at 1 nA. (c, d) SEM images of the particles after delithiation corresponding to plots a and b, respectively. Scale bar is 5 μm.

polishing before taking SEM images. The ion beam was only turned on during FIB polishing; the electron beam was only turned on during SEM imaging. The galvanostatic mode was used in all cycling with a voltage window between 0.01 and 1.5 V.

Figure 1 shows the microstructural evolution results for germanium particles cycled at different current rates. Figure 1a–d shows the voltage profiles of particles cycled at 0.12, 0.3, 1, and 3 nA (about 0.1, 0.21, 0.8, and 7.5 C rate), respectively. For the particle cycled at 0.12 nA, one large crack appeared on the surface after lithiation (Figure 1i). After delithiation, no more cracks or pores are shown on the surface (Figure 1m). Figure S2 shows the SEM images corresponding to the time points in Figure 1a. No nanopores or internal cracks appeared during delithiation. Previous XRD studies have shown that Ge particles go through a complete and homogeneous transformation from crystalline Ge to crystalline $Li_{15}Ge_4$ at a low C rate. We believe that the particle was fully lithiated to crystalline $Li_{15}Ge_4$ after 0.12 nA lithiation. The volume expansion was large enough to generate a crack on the particle. For the particle cycled at 0.3 nA, one small crack appears on the surface after lithiation (indicated by the arrow in Figure 1j). At the end of delithiation, both nanopores and cracks appeared on the polished surface (Figure 1n). Figure S3 shows the SEM images corresponding to the time points in Figure 1b. The proposed reaction mechanism in ref 21 can be used to explain this result. At 0.3 nA current, a heterogeneous structure including both crystalline $Li_{15}Ge_4$ and amorphous Li_xGe was generated at the end of lithiation. The smaller volume expansion only led to a small crack on the surface. However, different volume contractions from different phases in the heterogeneous structure generated internal cracks during delithiation. The formation of nanopores is due to the aggregation of vacancies during lithium extraction. At 0.12 nA, vacancies could diffuse out of the particle without aggregation due to the low delithiation rate; therefore, no nanopores were formed.

When the current was increased to 1 nA, the polished surface was intact after lithiation (Figure 1k). We believe that it is mainly due to the low capacity and small volume expansion of the Ge particle at a high lithiation rate. At the end of delithiation, some nanopores and one crack appeared on the surface (Figure 1o). The crack could be the initial defect inside the particle. At this current, the Ge particle cannot be lithiated to $Li_{15}Ge_4$, and the final product is amorphous Li_xGe at the end of lithiation. So there were no internal cracks appearing after delithiation. The formation of nanopores is still due to the aggregation of vacancies. When the current was increased to 3 nA, the polished surface is intact at the end of lithiation and delithiation without cracks and nanopores (Figure 1l,p). Compared to the particles cycled at lower currents, the volume expansion and contraction of the particle cycled at 3 nA are very small. The particle was composed of an amorphous Li_xGe shell and a crystalline Ge core. Although structure integrity was maintained at a high current, only a small portion of the capacity of Ge can be utilized. These results of microstructure change can be used to explain the cycling performance of the Ge electrode reported in ref 21 with good cycling performance at low and high current rates but poor cycling performance at intermediate current rate.

In order to obtain further understanding of the relationship between microstructure evolution and cycling rate, we tested Ge particles with different lithiation and delithiation rates. Figure 2a shows the voltage profile of a Ge particle lithiated at 1 nA and delithiated at 3 nA. Figure 2c shows the SEM image of the particle after delithiation and nanopores appear on the

DOI: 10.1021/acsaem.9b00380
ACS Appl. Energy Mater. 2019, 2, 2441–2446

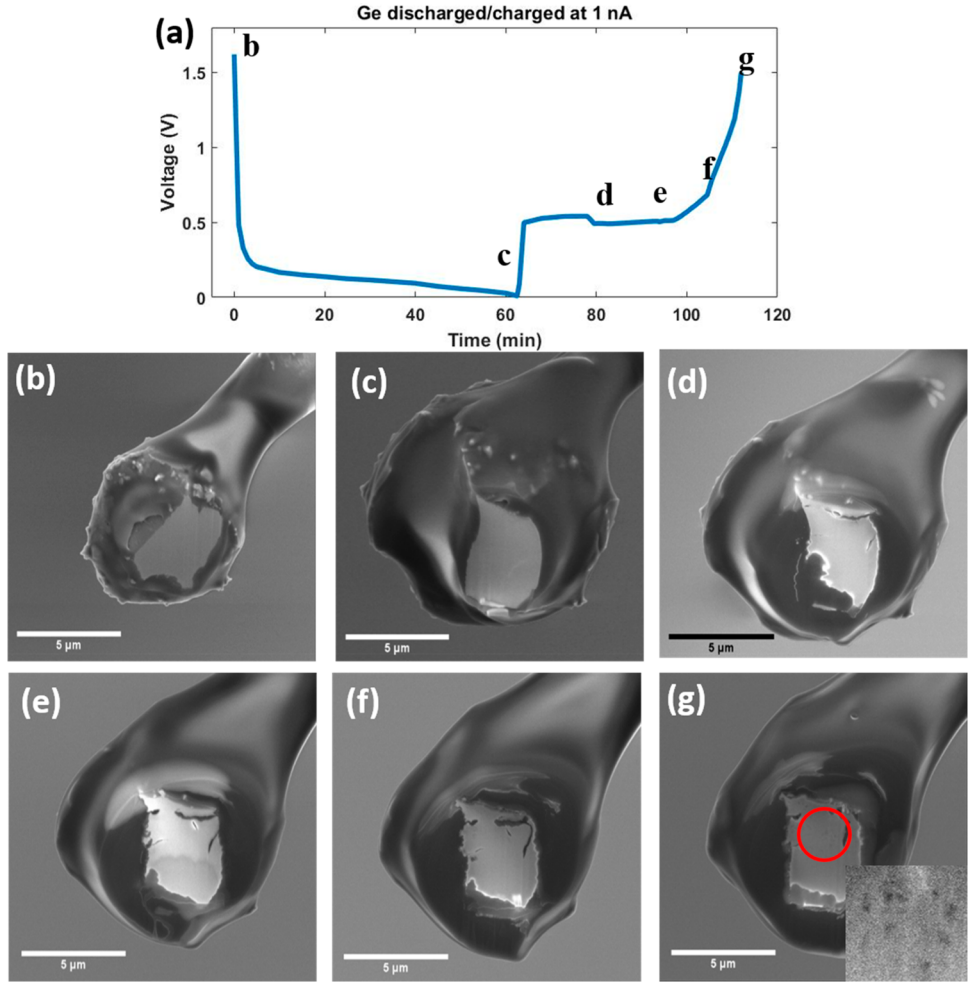

Figure 3. Ge particle cycled at 1 nA. (a) Voltage profile of the first cycle. (b) SEM image of as-prepared Ge particle. (c) SEM images of the same particle after lithiation. (d–g) SEM images at 30%, 60%, 80%, and 100% of delithiation states. Scale bar is 5 μm.

surface. Compared to the particle cycled at 3 nA shown in Figure 1p, this particle has a lower lithiation rate but the same delithiation rate. Nanopores appeared on the particle with the lower lithiation rate, but not at the other rate. During lithiation, lower lithiation rates can result in a higher lithium concentration in the particle and the larger volume expansion. This result indicates that lithium concentration has an impact on the formation of nanopores. At the same delithiation rate, the Ge particle with higher lithium concentration is more likely to form nanopores. Figure 2b shows the voltage profile of another Ge particle lithiated at 0.1 nA and delithiated at 1 nA. Figure 2d shows the SEM image of the particle after delithiation and nanopores appeared on the surface. This particle has a similar lithiation rate with the one cycled at 0.12 nA shown in Figure 1a,e,i,m, but with a higher delithiation rate. This result demonstrates that the delithiation rate also affects the nanopore formation. With the same lithium concentration, a higher delithiation rate is more likely to form nanopores. This conclusion is in accordance with the results reported in ref 28 which shows that the formation of a nanoporous structure during delithiation is related to the size of the particle, the lithium concentration, and the current rate.

To understand when the nanopores start to form, SEM images were taken at different states of charge during delithiation. Figure 3a shows the voltage profile of a Ge particle cycled at 1 nA; the SEM images were taken at points d–g, about 30%, 60%, 80%, and 100% of the delithiation process, which are shown in Figure 3d–g. The SEM images of fresh and lithiated particle are shown in Figure 3b,c. The surface was intact at the end of lithiation (point c). As shown in Figure 3d–f, the volume of the particle shrinks continuously. A few cracks appeared on the surface, but no nanopores are observed. The cracks could be the initial defects inside the Ge particle or generated during lithiation. At the end of delithiation (point g), some nanopores appeared on the surface as shown in the circled area in Figure 3g. This result shows that the nanopores only appear at the end of the delithiation process when amorphous Li_xGe is transformed to amorphous Ge.

To investigate the distribution of nanopores, a Ge particle cycle at 1 nA for 1 cycle was transferred to a TEM grid and FIB-SEM tomography was conducted. Video S1 shows that the nanopores are uniformly distributed inside the whole particle. This is a good indication that the polishing and imaging processes on the surface do not have an impact on the nanopore formation. In order to obtain a high-resolution image of the nanopores, a TEM specimen was obtained from the particle shown in Video S1. A JEOL JEM2100F TEM was employed for the microstructure analysis. Figure 4a is a low-magnification micrograph of the sample. Figure 4b is a TEM image of the porous structure circled in Figure 4a. Figure 4c,d are high-resolution TEM (HREM) images of nanopores. The

DOI: 10.1021/acsaem.9b00380
ACS Appl. Energy Mater. 2019, 2, 2441–2446

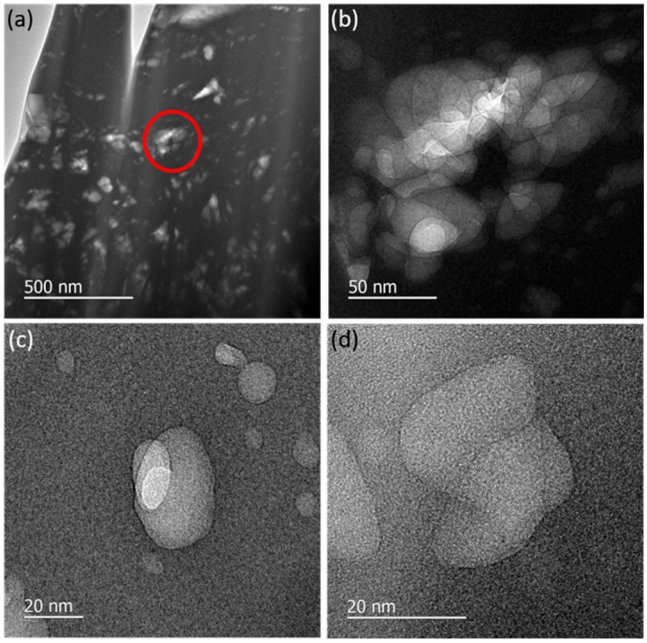

Figure 4. (a) TEM image of a Ge particle cycled at 1 nA after FIB thinning. (b) TEM image of the circled area in part a. (c, d) HREM images of nanopores.

TEM image shows the uniform distribution of nanopores inside the particle, and the size of the nanopores are in a range from several nanometers to around 100 nm. Figure 4c,d also shows that the crystalline Ge became amorphous after 1 nA (about 1 C) cycling.

To better understand the pulverization of a Ge electrode after cycling, we tested a Ge particle for 20 cycles at 0.7 nA (about 1 C rate). Figure S4a shows the cycling performance. The discharge capacity varied between 0.6 and 0.75 nAh, which could be caused by the microstructural change. After 20 cycles, FIB-SEM tomography was conducted. Some representative SEM images are shown in Figure S4b–d, and the 3D reconstruction is shown in Video S2. In Figure S4b, the particle is slightly polished on the edge, and some Ge nanowires appear on the surface. Figure S4c,d shows images after further polishing; nanowires still appear on the edge of particle. The reason could be the more complete lithiation and delithiation on the surface, which has a larger volume change than the internal part of the particle. Figure S4c,d also shows nanopores in the particle. Some nanopores remain isolated, but others merge together into large porous structures. Some porous structures are connected to the surface of the particle and act like cracks. They let ionic liquid electrolyte infiltrate into the particle and increase the active surface area. This may cause the capacity increase shown in the cycling performance. However, as cycling goes on, the porous structures will keep growing and eventually cause complete pulverization of particle, leading to a sudden failure of the Ge electrode.

In summary, our results show the relationship between cycling rate and microstructure evolution for a single Ge particle. At a low C rate like 0.1 C, no porous structure appears after delithiation. At intermediate C rates like 0.2 C, both internal cracks and nanopores appear after delithiation. When the C rate is increased to 0.8 C, only nanopores appear after delithiation. Upon a further increase of the C rate to 7.5 C, the particle remains intact after the first cycle. Nanopore formation is related to lithium concentration and delithiation rate. High lithium concentration and delithiation rate result in the formation of nanopores. Nanopores do not recover during cycling; they aggregate into large porous structures which could lead to particle pulverization and capacity fading of the Ge electrode.

■ ASSOCIATED CONTENT

Supporting Information

The Supporting Information is available free of charge on the ACS Publications website at DOI: 10.1021/acsaem.9b00380.

Ge particle cycled at 1 nA (AVI)
Ge particle cycled at 0.7 nA for 20 cycles (AVI)
Schematic of experimental setup and SEM images of Ge particles at different states of charge (PDF)

■ AUTHOR INFORMATION

Corresponding Authors

*E-mail: yuziliu@anl.gov (Y.L.).
*E-mail: likzhu@iupui.edu (L.Z.).

ORCID

C. Buddie Mullins: 0000-0003-1030-4801
Likun Zhu: 0000-0002-6324-3718

Notes

The authors declare no competing financial interest.

■ ACKNOWLEDGMENTS

This work was supported by the US National Science Foundation under Grants CBET-1603847 (L.Z.) and CBET-1603491 (C.B.M.). C.B.M. also gratefully acknowledges support from the Robert A. Welch foundation through Grant F-1496. This work was performed, in part, at the Center for Nanoscale Materials, an Office of Science user facility, and was supported by the U.S. Department of Energy, Office of Science, Office of Basic Energy Sciences, under Contract DE-AC02-06CH11357.

■ REFERENCES

(1) Armand, M.; Tarascon, J. M. Building better batteries. *Nature* **2008**, *451*, 652.
(2) Manthiram, A. Materials challenges and opportunities of lithium ion batteries. *J. Phys. Chem. Lett.* **2011**, *2* (3), 176–184.
(3) Goodenough, J. B. Electrochemical energy storage in a sustainable modern society. *Energy Environ. Sci.* **2014**, *7* (1), 14–18.
(4) Obrovac, M. N.; Christensen, L. Structural Changes in Silicon Anodes during Lithium Insertion/Extraction. *Electrochem. Solid-State Lett.* **2004**, *7* (5), A93–A96.
(5) Nitta, N.; Yushin, G. High-Capacity Anode Materials for Lithium-Ion Batteries: Choice of Elements and Structures for Active Particles. *Particle & Particle Systems Characterization* **2014**, *31* (3), 317–336.
(6) Goriparti, S.; Miele, E.; De Angelis, F.; Di Fabrizio, E.; Proietti Zaccaria, R.; Capiglia, C. Review on recent progress of nanostructured anode materials for Li-ion batteries. *J. Power Sources* **2014**, *257*, 421–443.
(7) Tian, H.; Xin, F.; Wang, X.; He, W.; Han, W. High capacity group-IV elements (Si, Ge, Sn) based anodes for lithium-ion batteries. *Journal of Materiomics* **2015**, *1* (3), 153–169.
(8) Graetz, J.; Ahn, C.; Yazami, R.; Fultz, B. Nanocrystalline and thin film germanium electrodes with high lithium capacity and high rate capabilities. *J. Electrochem. Soc.* **2004**, *151* (5), A698–A702.
(9) Chou, C.-Y.; Hwang, G. S. On the origin of the significant difference in lithiation behavior between silicon and germanium. *J. Power Sources* **2014**, *263*, 252–258.

DOI: 10.1021/acsaem.9b00380
ACS Appl. Energy Mater. 2019, 2, 2441–2446

(10) Kennedy, T.; Brandon, M.; Ryan, K. M. Advances in the Application of Silicon and Germanium Nanowires for High-Performance Lithium-Ion Batteries. *Adv. Mater.* **2016**, *28* (27), 5696−5704.
(11) Kennedy, T.; Mullane, E.; Geaney, H.; Osiak, M.; O'Dwyer, C.; Ryan, K. M. High-Performance Germanium Nanowire-Based Lithium-Ion Battery Anodes Extending over 1000 Cycles Through in Situ Formation of a Continuous Porous Network. *Nano Lett.* **2014**, *14* (2), 716−723.
(12) Chan, C. K.; Zhang, X. F.; Cui, Y. High Capacity Li Ion Battery Anodes Using Ge Nanowires. *Nano Lett.* **2008**, *8* (1), 307−309.
(13) Park, M.-H.; Kim, K.; Kim, J.; Cho, J. Flexible Dimensional Control of High-Capacity Li-Ion-Battery Anodes: From 0D Hollow to 3D Porous Germanium Nanoparticle Assemblies. *Adv. Mater.* **2010**, *22* (3), 415−418.
(14) Park, M.-H.; Cho, Y.; Kim, K.; Kim, J.; Liu, M.; Cho, J. Germanium Nanotubes Prepared by Using the Kirkendall Effect as Anodes for High-Rate Lithium Batteries. *Angew. Chem., Int. Ed.* **2011**, *50* (41), 9647−9650.
(15) Wu, S.; Han, C.; Iocozzia, J.; Lu, M.; Ge, R.; Xu, R.; Lin, Z. Germanium-Based Nanomaterials for Rechargeable Batteries. *Angew. Chem., Int. Ed.* **2016**, *55* (28), 7898−7922.
(16) Liu, X. H.; Huang, S.; Picraux, S. T.; Li, J.; Zhu, T.; Huang, J. Y. Reversible Nanopore Formation in Ge Nanowires during Lithiation-Delithiation Cycling: An In Situ Transmission Electron Microscopy Study. *Nano Lett.* **2011**, *11* (9), 3991−3997.
(17) Chan, M. K. Y.; Long, B. R.; Gewirth, A. A.; Greeley, J. P. The First-Cycle Electrochemical Lithiation of Crystalline Ge: Dopant and Orientation Dependence and Comparison with Si. *J. Phys. Chem. Lett.* **2011**, *2* (24), 3092−3095.
(18) Silberstein, K. E.; Lowe, M. A.; Richards, B.; Gao, J.; Hanrath, T.; Abruña, H. D. Operando X-ray Scattering and Spectroscopic Analysis of Germanium Nanowire Anodes in Lithium Ion Batteries. *Langmuir* **2015**, *31* (6), 2028−2035.
(19) Lim, L. Y.; Fan, S.; Hng, H. H.; Toney, M. F. Operando X-ray Studies of Crystalline Ge Anodes with Different Conductive Additives. *J. Phys. Chem. C* **2015**, *119* (40), 22772−22777.
(20) Jung, H.; Allan, P. K.; Hu, Y.-Y.; Borkiewicz, O. J.; Wang, X.-L.; Han, W.-Q.; Du, L.-S.; Pickard, C. J.; Chupas, P. J.; Chapman, K. W.; Morris, A. J.; Grey, C. P. Elucidation of the Local and Long-Range Structural Changes that Occur in Germanium Anodes in Lithium-Ion Batteries. *Chem. Mater.* **2015**, *27* (3), 1031−1041.
(21) Lim, L. Y.; Fan, S.; Hng, H. H.; Toney, M. F. Storage Capacity and Cycling Stability in Ge Anodes: Relationship of Anode Structure and Cycling Rate. *Adv. Energy Mater.* **2015**, *5* (15), 1500599.
(22) Liu, X. H.; Liu, Y.; Kushima, A.; Zhang, S.; Zhu, T.; Li, J.; Huang, J. Y. In Situ TEM Experiments of Electrochemical Lithiation and Delithiation of Individual Nanostructures. *Adv. Energy Mater.* **2012**, *2* (7), 722−741.
(23) Liang, W.; Yang, H.; Fan, F.; Liu, Y.; Liu, X. H.; Huang, J. Y.; Zhu, T.; Zhang, S. Tough Germanium Nanoparticles under Electrochemical Cycling. *ACS Nano* **2013**, *7* (4), 3427−3433.
(24) Liu, Y.; Zhang, S.; Zhu, T. Germanium-Based Electrode Materials for Lithium-Ion Batteries. *ChemElectroChem* **2014**, *1* (4), 706−713.
(25) Weker, J. N.; Liu, N.; Misra, S.; Andrews, J. C.; Cui, Y.; Toney, M. F. In situ nanotomography and operando transmission X-ray microscopy of micron-sized Ge particles. *Energy Environ. Sci.* **2014**, *7* (8), 2771−2777.
(26) Zhou, X.; Li, T.; Cui, Y.; Fu, Y.; Liu, Y.; Zhu, L. In Situ Focused Ion Beam Scanning Electron Microscope Study of Microstructural Evolution of Single Tin Particle Anode for Li-Ion Batteries. *ACS Appl. Mater. Interfaces* **2019**, *11* (2), 1733−1738.
(27) Klavetter, K. C.; Pedro de Souza, J.; Heller, A.; Mullins, C. B. High tap density microparticles of selenium-doped germanium as a high efficiency, stable cycling lithium-ion battery anode material. *J. Mater. Chem. A* **2015**, *3* (11), 5829−5834.
(28) Chen, Q.; Sieradzki, K. Spontaneous evolution of bicontinuous nanostructures in dealloyed Li-based systems. *Nat. Mater.* **2013**, *12*, 1102.

DOI: 10.1021/acsaem.9b00380
ACS Appl. Energy Mater. 2019, 2, 2441−2446